

# 'Traffic Light' Theory for Covid-19 Spatial Mitigation Policy Design

**Michael Beenstock**

Department of Economics, Hebrew University of Jerusalem

**Daniel Felsenstein**

Department of Geography, Hebrew University of Jerusalem

**Xieer Dai**

College of Economics, University of Shenzhen

## **Abstract**

We suggest the use of outdegrees from graph theory to rank locations in terms of their contagiousness. We show that outdegrees are equal to the column sums of spatial autoregressive matrices, which may be estimated using econometric methods for spatial panel data. Outdegree is a superior concept to  $R$  for 'traffic light' shading because it distinguishes between the export and import of contagion between locations. Simulation methods are used to illustrate the concept of outdegrees and its structural determinants in terms of centrality, indigenous contagion and spatial contagion. A secondary criteria for traffic light shading involves the stochastic structure of morbidity shocks, which induce 'spiking' through their autoregressive persistence, conditional heteroscedasticity and diffusion jump parameters.

## 1. Introduction

From the outset the Covid-19 epidemic has been characterized by its spatial or geographic heterogeneity. In some locations within countries the epidemic has been particularly intense, while in others it has been mild and even non-existent. In an attempt to control the pandemic, national governments have adopted 'traffic light' policies, which differentiate lockdown measures across locations according to the intensity of their Covid-19 morbidities and recovery performance. Spatial units such as neighborhoods, cities or regions are assigned a Covid-19 performance score that is color coded according to traffic light colors. Seemingly arbitrary cut-off points determine the move from color to color. As Covid-19 outcomes rise or wane, locations find themselves moving across the different categories with their attendant lockdown or travel restrictions. In essence, traffic light policy is a tool for operationalizing spatially differentiated mitigation policy.

Traffic light policy in practice (reviewed in section 2) highlights the arbitrariness in determining color changes in traffic light policy formulation. There is little common use of variables or criteria for assigning color codes and in the absence of any standardized measure for change, each country developed its own (often opaque) method. Furthermore, many of the countries that adopted a traffic light system for the spatial mediation of Covid-19 ignore the challenges of calculating a spatially-sensitive  $R$ . In this paper we argue that while it is relatively straightforward to calculate  $R$  nationally, matters are very different when  $R$  is location specific. This difference arises because locations import and export Covid-19 to each other through human contact and economic and social intercourse between them. The same phenomena are much weaker at the international level than at the intranational level because it is much easier to control cross-border movements between countries than within them, and the scale of cross-border traffic is much greater intra-nationally than internationally.

We argue that operationalizing spatial mitigation policy by calculating  $R$  for locations using the same methods as for countries is likely to produce accident-prone traffic lights. Green locations might be mistaken for red, and red for green. Just because Covid-19 morbidity happens to be increasing in some location does not mean that its  $R$  is greater than 1. By the same token, just because Covid-19 morbidity happens to be decreasing does not mean that its  $R$  is less than 1.

To ensure that such errors do not arise, we propose a new methodology for ranking the contagiousness of different locations in terms of their outdegrees from graph theory (Diestel 2005). Outdegree measures the effect of a random increase in morbidity in a given location on morbidity in all other locations, and replaces the use of both R and arbitrary weighting systems. Locations with the largest outdegrees are color coded 'red' while locations with the smallest outdegrees are color-coded 'green'. Under this regime local imports and exports of Covid-19 are linked in a closed system. If an area increases its imports of Covid-19 then by definition other areas must be exporting more. As traffic light policy works on the basis of ranks, locations can increase the volume of Covid-19 exporting activity and still maintain the same rank. Since outdegrees are equivalent to column sums of spatiotemporal impulse response matrices, they may be estimated by econometric methods designed for nonstationary spatial panel data (Beenstock and Felsenstein 2019).

This paper proceeds as follows. Section 2 reviews the literature on spatial mitigation policy for Covid-19. In section 3 we present a stochastic SIR model in discrete time, which is amenable to estimation using econometric methods for spatial panel data. Section 4 illustrates how outdegrees are derived from SIR models, and how they distinguish between indigenous and imported contagion. In section 5 we compare contagion heat maps based on outdegrees with R-based contagion patterns derived for synthetic locations and highlight the superior performance of the former. Section 6 considers the role of 'spikes' in the coloring of traffic light policy. Since spiking is not randomly distributed across locations, it fattens the right-hand tails of morbidity distributions, which darken their color coding in traffic light terms. Finally, despite our theoretical and conceptual focus, we conclude with a discussion of empirical implementation and likely policy implications in Section 7.

## **2. Spatial Mitigation Policy for Covid-19**

In principle, lockdown policy for controlling pandemics runs along a continuum ranging from spatial targeting (of neighborhoods, quarters commuting zones, cities and regions) through to uniform, one-size-fits-all measures with no spatial differentiation. In practice, the practicalities of implementation and interest-group pressures reduce the range of mitigation measures available to policy makers. Proposals for zone-based lockdowns are invariably based on existing administrative

units such as postal codes, statistical areas or communes (Monras 2020, Olliu-Barton et al 2020). To operationalize targeted mitigation policies, law enforcement agencies need to translate non-intuitive zoning schemes into demarcated territories 'on the ground'. This is not always practicable, especially as not every zone is self-contained in terms of critical health and welfare services to accommodate even short-term closure.

Uniform lockdown policies similarly suffer from political pressures to absolve individual sectors or segments of the population or from inconsistent implementation as policy enforcement suffers erosion over successive pandemic waves (Warren et al 2020). Given that many of the proposed policy measures for constraining labor and population mobility have never been implemented before, their economic and social costs are effectively unknown.

#### *Traffic Light Policy in Practice*

The European Center for Disease Control produces weekly traffic light maps at the NUTS2 level in an attempt to co-ordinate travel restrictions across EU member states (ECDC 2021). This system uses four color labels (green, orange, red and dark red) to classify travel risk areas across the EU based on two common variables: the 'notification rate' defined as the total newly notified Covid-19 cases per 100 000 population over the previous 2 weeks, and the 'test positivity rate' defined by the percentage of positive tests across all Covid-19 tests over the previous week. Traffic light color changes are determined by administratively determined cut-offs<sup>1</sup>.

The British government operates a 4-tier strategy to control the spread of Covid-19 while differentiating across locations. Local restrictions are imposed on a complicated mix of geographies varying from counties, unitary authorities, combined authorities to London boroughs (Cheshire and Singleton 2020). The four-tier system ranges from Tier 1 (Medium Alert) to Tier 4 (Stay at Home). Key epidemiological indicators for measuring the intensity of the epidemic and moving across tiers include case detection

---

<sup>1</sup> The cut off values are for notification rate (*nr*) and test positivity rate (*tp*) are: green=  $nr < 25$  and  $tp < 4\text{percent}$ ; orange= $nr < 50$  and  $tp > 4\text{percent}$  or  $25 < nr < 150$  and  $tp < 4\text{percent}$ ; red= $nr > 50$  and  $tp > 4\text{percent}$  or  $nr > 150$  and dark red= $nr > 500$ .

The choice of the cut-off values for *nr* and *tp* is nowhere justified. It is likely that they are the result of political negotiation: the original proposal for a coordinated response for restricting free movement suggested more stringent values: <https://eur-lex.europa.eu/legal-content/EN/TXT/?qid=1604080584943&uri=CELEX%3A52020DC0499>

rates in all age groups, case detection rates in the over-60s, rates of change in these indicators, the test positivity rate, and the pressure on the public health system. Again, the relative weights of these factors are not formalized and the criteria for movement through the different levels are consequently impressionistic and opaque<sup>2</sup>.

In New Zealand the government uses a four-level alert system to institute different degrees of lockdown and mitigate mobility (NZGOV 2020). At each level, measures get progressively more restrictive. Thus Level 1 indicates that the disease is contained locally but not nationally. Level 2 denotes that while the pandemic is contained a risk of community transmission exists. At Level 3 there is a high risk that the disease is not contained and this evokes an appropriate range of lockdown and distancing measures. Finally, at Level 4 widespread outbreaks and transmission occur that call for stringent constraints on mobility and social interaction. However, these alert levels are national in nature and are not spatially differentiated across the 20 District Health Boards which serve as the units for the regional management of Covid-19.

In France a five-level alert system exists (Connexion France 2020). The countries' 102 Departments are classified into 5 zones ranging from green (clean) areas through alert zones, heightened alert zones, maximum alert zones and state of health emergency zones. The intensity of the pandemic in different locations is measured by morbidity rates, level of contagion amongst the elderly and impact on intensive care facilities.

Israel uses a four-tiered, color-coded, traffic light system for operationalizing spatially differentiated lockdown (MoH 2020a). The basic spatial unit for mitigation policy is the city or local authority with some of the largest cities subdivided into neighborhoods. Each spatial unit is awarded a numerical epidemic intensity score based on a transparent formula. Cities are assessed bi-weekly and assigned color codes ranging from green through yellow and orange to red, corresponding to different levels of lockdown stringency<sup>3</sup>.

---

<sup>2</sup> The arbitrary nature of this tier-based allocation is reflected in written statement to Parliament by the Minister of Health and Social Care: "while each metric is important in its own right, the interplay between each indicator for a given area is equally important, so a hard and fast numerical threshold on each metric is not appropriate". (GOVUK 2020)

<sup>3</sup> The formula used for assigning places to color codes is publicly available (MoH 2020b). Each spatial unit  $i$  is assigned an intensity score ( $S$ ) defined as:

Color coding has not been static and Covid-19 locational intensities tend to vary over time. 'Red' locations can turn 'green' and vice-versa. Using data for some 2000 statistical areas in Israel, we have constructed dynamic maps of the spread of the epidemic, which show that traffic light colors vary considerably. They also show that as of July 2021 40 statistical areas remained 'Covid clean' (see HUGIS 2020).

As Covid-19 is about local contagion it makes sense to design spatial mitigation policy at the most granular level of resolution available. For example, Israeli mitigation policy in the first-wave of Covid-19 was designed nationally and lockdown and related mitigation policies were applied nationwide. To measure national intensity of the epidemic,  $R_e$ , the effective reproduction rate was invariably used. In subsequent waves, mitigation policy increasingly had a geographic design in recognition of the spatial heterogeneity of the epidemic. The so-called 'traffic light' system aims to apply mitigation policy differentially across locations.

### *Literature Review*

A variety of methodological approaches to assessing the role of mobility restrictions for mitigating Covid-19 transmission has been attempted at different spatial scales and in diverse national contexts. For example, using time series data Wieland (2020)

$$S_i = k + \ln(N_i \times G_i^2) + \frac{P_i}{m}$$

where:  $N_i$  = number of new infectives per 10,000 population in local authority  $i$ ,  $P_i$  denotes the amount of new positive tests conducted in each local authority over the previous week,  $G_i$  is the growth rate of infectees over the previous week and  $m$  and  $k$  are scaling constants ensuring  $0 < S < 10$ .

However, there are various problems with this formula:

1. It doubles counts new cases as  $N=P/T$  where  $T$  is the number of tests. If  $T$  increases for administrative reasons,  $P$  will tend to decrease which may artificially reduce  $S$
2. Suppose  $P$  happens to be large because of efficient referrals or  $P$  happens to be small because people decide they do not want to be tested. The formula penalizes efficiency and rewards tardiness.
3. The role of  $G^2$  implies that  $S$  will be smaller in a place where  $N$  is large but decreasing, than where  $N$  is small but increasing. This may lead to absurd results in which hotspots are green and coldspots are red.
4.  $S$  is not defined when  $N=0$  because  $\ln(0)$  is not defined. In these cases,  $S$  may be 0. If  $N$  is very large but decreasing,  $S$  may be low so that traffic light colors will change from red directly to green.

estimates spatial growth models for Covid-19 mortality across German counties. He finds a temporal mismatch between mortality trends and the implementation of mitigation measures. This raises questions as to the causal effect of mitigation policies and suggests that identification issues can undermine some of the claims attributed to spatial mitigation policy.

In contrast, Gatto et al (2020) use a spatially explicit simulation model calibrated for Italian provinces to test scenarios for different pandemic containment measures. Their results suggest that mobility restrictions can reduce Covid-19 contagion by 42-49 percent. More conservative estimates using a very different method are presented by Glaeser et al (2020). They use spatial panel data for New York at the zip code level to test the effect of mobility reductions on Covid-19 controlling for differences in testing rates and the concern that testing increases mobility as people travel to test centers. Their estimations point to a 10 percent reduction in mobility leading to a 30 percent decrease in Covid-19 morbidity.

Much recent work related to spatial mitigation policy is concerned with optimization. Giannone et al (2020) combine a spatial SEIR model with an interregional trade model and calibrate the effect of mobility restrictions on national welfare using state level data on Covid-19 morbidity in the US. They compare spatially targeted and spatially uniform lockdown measures and highlight the optimal policy combination that integrates within-state and between-state restrictions. Their findings emphasize the effectiveness of local containment combined with astute timing. They also find that restricting trade and mobility across states reduces welfare losses but not the mortality rate. Consequently, they advocate a combined strategy of local lockdown with travel restrictions.

In another calibrated study, Fajgelbaum et al (2020) investigate optimal lockdown over time and space in a commuting network. They too integrate a spatial epidemiological and trade model. In their framework the epidemic is transmitted through the interactions of commuters at their workplaces. Infected workers from one location infect susceptible residents from another location at third-party workplace locations. Containment policies such as lockdown, directly reduce the income of workers who stay at home and indirectly affect other locations through shifts in expenditures. Fajgelbaum et al (2020) simulate optimal lockdowns across the

continuum ranging from spatially targeted to uniform measures. They calibrate their model using commuting and cellphone data for New York, Seoul and Daegu, and compare optimal pandemic policies with observed commuting responses. Their results highlight the benefits of spatial targeting and underscore the effect of this policy on mitigating real income losses.

Argente et al (2020) use a SIR model with multiple sub-populations and a model of commuting choice between sub-populations to calibrate a Covid-19 lockdown in Seoul. Uniquely and contravertially, the South Korean government publicly discloses data on Covid-19 infectees as part its mitigation policy. They study the strategy of information disclosure to the alternatives of information non-disclosure and uniform lockdown. They find that the change in commuting patterns induced by the policy of public disclosure considerably reduces morbidity and mortality, and it reduces economic costs by a factor of four compared to the alternative of uniform lockdown. Similar hybrid optimization models for lockdown policy that combine a (spatial-epidemiological) SIR model with a trade/commuting economic model can be found in recent research by Alvarez et al (2020) and Birge et al (2020).

In contrast to the ODE (ordinary differential equations) approach that underpins many of the SIR-type models, Zhu et al 2017, Prem et al 2020 and Yamamoto et al (2021) use partial differential equation modeling (PDE) to quantify compliance with Covid-19 mitigation policies at the regional level in the US. This involves setting up a spatio-temporal model of Covid19 contagion that maintains a spatial balance in which the rate of Covid change in a region equals the rate at which it flows across regions plus the rate at which it is created or destroyed within regions. In this way, the formulation admits 'trade' in Covid-19 transmission distinguishing between global (inter-regional) and local (intra-regional) processes. However, the representation of regions as a string of continuous, single-dimension points along an axis in Euclidean space and the coarse granularity of the 10 supra-regions, arguably serve to dilute any meaningful insights with respect to mitigation policy at the local level.

In summary, recent studies conclude that spatially differentiated mitigation policy is superior to nationwide mitigation policy. Perhaps this result was obvious in the first place. The main practical problem remains how to implement spatially differentiated policy. Since these studies are based on calibration, their policy suggestions are



inevitably sensitive to calibration error, induced by indirect inference. Empirical test statistics for indirect inference of calibrated DSGE (dynamic stochastic general equilibrium) macroeconomic models have shown (Meenagh et 2019) that they are overwhelmingly rejected by naïve VAR models. If the same applies to calibrated spatial models of Covid-19 contagion, we suggest that the design of spatially differentiated mitigation policy be based on spatial models estimated by direct inference. Specifically, we suggest the use of direct rather than indirect inference using econometric methods for dynamic spatial panel data.

### **3. A Discreet Spatial SIR Model**

Recent work incorporating spatial econometrics in the analysis of Covid-19 contagion, illustrates the potential inherent in this approach (Krisztin et al 2020, Mitze and Kosfeld 2021, Wieland 2020). We extend current work by using spatial econometrics to handle multilateral resistance (Anderson and Van Wincoop 2003) in spatial networks of mutual contagion.

#### *Terminology*

We begin by introducing some terminology. A 'domain' is a geographic area such as a country or a state or province within it. Space is more 'granular' if the domain comprises a larger number of separate locations (granules). 'Infill asymptotics' arises when the number of granules tends to infinity for a given domain. 'Expanding domain asymptotics' arises when the domain tends to infinity for a given granule (node) size. Granules or locations may be regarded as 'nodes' in a network. A 'directed graph' depicts the connectivity between nodes. In the absence of connectivity, nodes are 'insular'. In 'star networks' all nodes are connected to a central nucleus but otherwise are not mutually connected. In 'complete networks' all pairs of nodes are connected. 'Network centrality' refers to the asymmetric importance of nodes in the network as measured by their 'outdegrees'. Outdegrees measure the salience of nodes in the network.

We shall argue that outdegrees measure the contagiousness of locations and therefore constitute the primary criterion for color coding traffic light policy. We shall also argue that the greater the asymmetry induced by network centrality, the fatter are the tails of the distribution of outcomes (morbidity) in the network. Indeed, the Lindeberg condition of the celebrated central limit theorem breaks down if there is too much

network centrality. It breaks down totally in star networks (Acemoglu et al 2012) in which event 'black swans' in the tail affect the moments of the distribution; the tail wags the dog. In the context of Covid-19 these black swans are super-spreaders.

In summary, in the absence of network centrality individual granules cannot affect the shape of the sand-pile; they are too small to matter. They might not matter even if there is limited dependence in the network. At the other extreme the nuclei of star networks are too big not to matter; what happens to them causes the sand-pile to collapse. Their outdegree is infinite induced by chain reaction within the network. As we shall see, size is not necessarily physical; it is measured by outdegree.

### *SIR Model*

Let  $y_t$  denote an  $N$ -vector of Covid-19 morbidity during time period  $t$  (e.g. daily, weekly positive diagnoses) where  $N$  denotes the number of locations in the domain. Let  $k_t$  denote an  $N$ -vector of infectives at the beginning of period  $t$ . Let  $W$  denote an  $N \times N$  connectivity matrix between locations with elements  $w_{jh}$  where  $w_{jj} = 0$  and with  $\sum_{h \neq j}^N w_{jh} = 1$ , i.e. the leading diagonal of  $W$  is zero and  $W$  is row-summed to 1 for purposes of normalization. The basic first-order spatiotemporal model for  $y_t$  may be written as

$$y_t = \Lambda y_{t-1} + \Gamma W y_t + \Pi k_t + \Psi W k_t + \varepsilon_t \quad (1)$$

where capital Greek symbols are  $N \times N$  diagonal matrices with, e.g, elements  $\lambda_j$  for  $\Lambda$ , which measure the temporal autoregressive component of  $y$ ,  $\gamma_j$  measures the spatial autoregressive component (SAR),  $\pi_j$  measure the infection rate in location  $j$  with respect to its own infectives, and  $\psi_j$  measures the infection rate in location  $j$  with respect to infectives elsewhere. Finally,  $\varepsilon > 0$  is an iid random  $N$ -vector measuring idiosyncratic morbidity. Notice that if  $\Gamma = \Psi = 0$  equation (1) reverts to a standard model of contagion in which each location is an island unto itself. Under such autarky estimates of  $\Lambda$  and  $\Pi$  may be used to calculate  $R_j$  because by definition there is no 'trade' in Covid-19.

We assume that recovery rates ( $0 < \delta < 1$ ) for infectives vary by location, hence:

$$k_t = \Phi k_{t-1} + y_{t-1} + e_{t-1} \quad (2)$$

where  $\Phi$  is an  $N \times N$  diagonal matrix with elements  $0 < 1 - \delta_j = \phi_j < 1$ , and  $e > 0$  is an iid homoscedastic  $N$ -vector of random shocks to recovery. When  $e = 1$  an existing infective does not recover, as a result of which the number of infectives ( $k$ ) increases by 1 directly, but the number diagnosed remains unchanged. Mean time to recovery is:

$$\tau = \sum_{i=0}^{\infty} i \phi^i = \frac{\phi}{(1-\phi)^2} \quad (3)$$

For example, if  $\tau$  is 2 weeks equation (3) implies  $\phi = 0.766$ ; the recovery rate ( $\delta$ ) is 0.233 per day. In summary, the model has two stochastic components related to morbidity ( $\varepsilon$ ) and delayed recovery ( $e$ ). These shocks are positive because morbidity and delayed recovery cannot be negative.

Equation (1) ignores 'removals', represented here by recoveries, which reduce the population of susceptibles. This simplification, made in the interest of linearity, is reasonable, especially in the early stages of an epidemic, but matters would be different when it enters its mature stage.

Equation (1) may be rewritten as:

$$y_t = G y_{t-1} + B k_t + A \varepsilon_t \quad (4)$$

where  $A = (I - \Gamma W)^{-1}$ ,  $G = A \Lambda$  and  $B = A(\Pi + \Psi W)$ . Equations (2) and (4) jointly determine the dynamics of  $y$  and  $k$ . The Wold representation for  $y$  is obtained by substituting equation (2) into equation (3) for  $k$ :

$$y_t = (\Phi + G + B) y_{t-1} - G \Phi y_{t-2} + A \varepsilon_t - A \Phi \varepsilon_{t-1} + B e_{t-1} \quad (5)$$

Equation (5) characterizes the spatiotemporal contagion for Covid-19 morbidity ( $y$ ). The second order temporal dynamics stem from the fact that current morbidity during period  $t$  depends on infectives at the start of period  $t$ , while the latter varies directly with morbidity in period  $t-1$ . Equation (5) generates a rich taxonomy for the transmission of Covid-19 morbidity shocks ( $\varepsilon$ ) and recovery shocks ( $e$ ) across locations and over time.

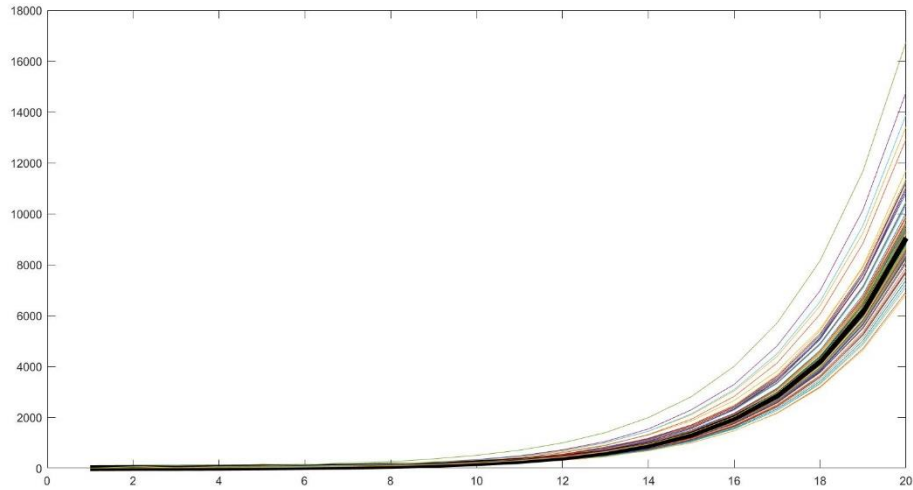
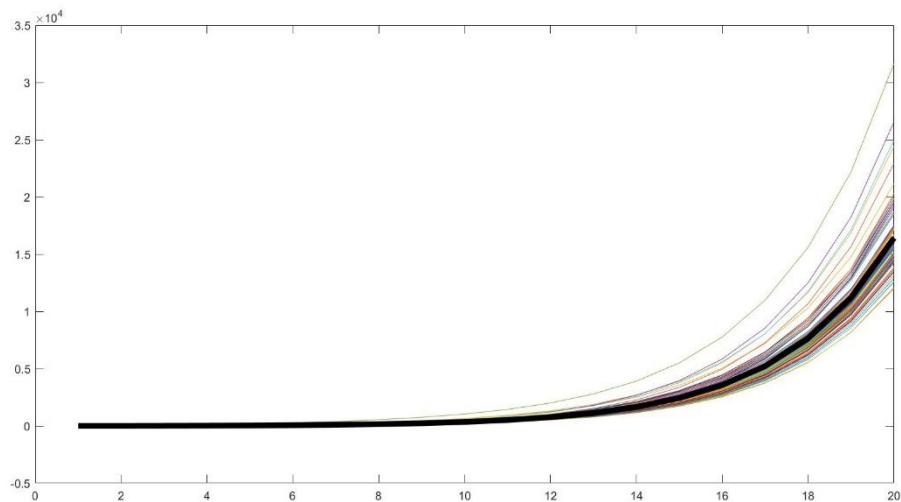
**Figure 1A Simulated Morbidity (y)****Figure 1B Simulated Infectives (k)**

Figure 1 simulates the dynamics of  $y$  and  $k$  for a domain represented by a  $10 \times 10$  square lattice (hence  $N = 100$ ) in which spatial dependence is based on first-order rook contiguity.  $W$  is row summed to unity inside the lattice, to  $2/3$  on its edge and to  $1/2$  in its corners. This normalization results from the fact that inside the lattice spatial units have four immediate rook neighbors, on the edge they have three, and in the corners, they have two. Therefore, spatial units differ in terms of their centrality.

However, they are otherwise homogeneous because they share the common parameters;  $\lambda = 0.3$ ,  $\gamma = 0.1$ ,  $\pi = 0.4$ ,  $\psi = 0.2$ , and  $\phi = 0.9$ . The initial conditions for  $y$  and  $k$  are zero (before the outbreak of Covid-19). The epidemic is initialized by randomly drawing  $\varepsilon$  in period 1 from a spatially independent homoscedastic lognormal distribution (to ensure that  $\varepsilon$  is not negative) for each spatial unit in the lattice. In period 2  $e$  and  $\varepsilon$  are drawn for each spatial unit. And so on until period  $T$ , which equals 20 in Figure 1. This history is repeated 1000 times, and the means of  $y$  and  $k$  are plotted in Figure 1.

Figure 1A is a 'spaghetti' graph in which the bold schedule plots the average value of  $y$  in each period, and the 100 other schedules plot the simulated panel data for  $y$ . Clearly,  $y$  is explosive because the choice of parameter values implies that  $R$  exceeds 1. This befits an epidemic in its early stages before 'removals' have a damping effect on the propagation of the epidemic. In period 20 average morbidity is close to 10,000. However, in some locations it is as high as 160,000 while in others it is as low as 7,000. These differences are induced by randomness in  $\varepsilon$  and  $e$  as well as differences in centrality as discussed below. Figure 1B shows a similar pattern at a different scale for simulated infectives.

Figure 2A plots the histogram for morbidity ( $y$ ) generated by Figure 1A in period 20. The distribution may be fat-tailed for two reasons. First, because  $\varepsilon$  and  $e$  have lognormal distributions, integrals of  $\varepsilon$  and  $e$  are skewed to the right. Second, as noted by Acemoglu et al (2012), star network effects, induced here by spatial dependence, generate right fat-tails.

Since the log counterpart of Figure 2A is not fat-tailed, only the first of these phenomena is present. However, when  $T$  is increased to 100 Figure 2A tends to have fatter tails. Furthermore, when  $W$  is defined in terms of inverse distance instead of rook-contiguity, the counterpart to Figure 2A is fatter tailed because inverse distance implies the network is complete whereas it is incomplete under contiguity.

**Figure 2A The Distribution of Morbidity after 20 Periods**

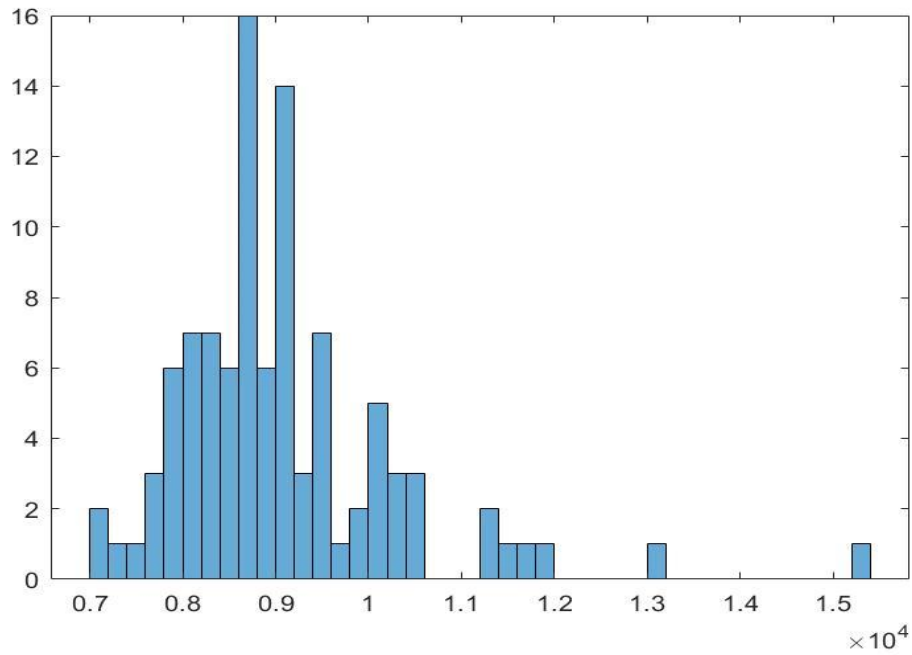
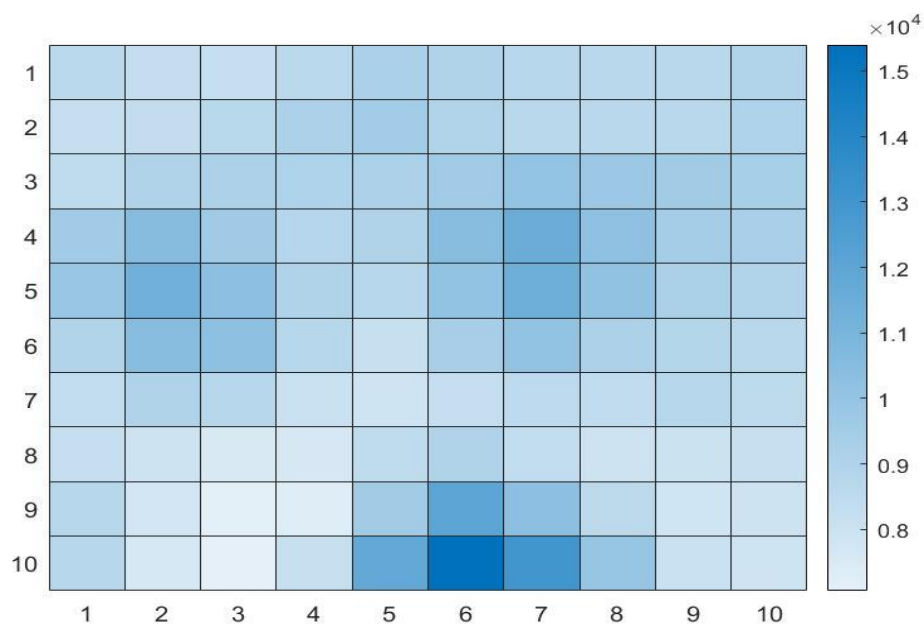


Figure 2B plots the heat map generated by Figure 2A in which tiles refer to their location in the lattice. The greatest morbidity in period 20 occurs in location with address row 10 column 6 (deep blue). Notice that the locations in the tail of Figure 2A are spatially clustered. There is also evidence of spatial clustering regarding locations in other parts of the distribution.

**Figure 2B Heat Map for Morbidity in Period 20**



#### 4. Spatial Mitigation Policy Using Outdegrees

In this section we use the spectral decomposition of a matrix to present an alternative method to R for ranking the contagiousness of locations. We rank them using outdegrees, measured by the columns sum of spatiotemporal propagation matrices derived from spatiotemporal contagion models such as equations (1) and (2).

Outdegrees measure the effect of a random increase in morbidity in a location on morbidity within this location as well as in all other locations. Outdegree therefore measures the global contagion generated by infectives in each location; it includes indigenous contagion as well contagion exported to other locations. By contrast, R calculated for locations does not distinguish between exported and imported contagion. We also present results of sensitivity tests for key model parameters and for different spatial geometries.

Setting  $\Lambda = \Gamma = 0$  in equation (1) greatly simplifies matters by making  $y$  recursive to  $k$  and implies the following first order spatiotemporal model for  $k$ :

$$k_t = \Omega k_{t-1} + v_{t-1} \quad (6)$$

where  $\Omega = \Phi + \Pi + \Psi W$  with elements  $\omega_{sn}$  and  $v = \varepsilon + e$ . The general solution for  $k$  is the Wold representation for equation (6):

$$k_t = \sum_{j=1}^{\infty} \Omega^{j-1} v_{t-j} \quad (7)$$

The  $s$ 'th column sum of  $\Omega^{j-1}$  measures the  $j-1$ 'th order outdegree for Covid-19 shocks in location  $s$  on all locations including  $s$ . When  $j = 2$  let  $\sum_{n=1}^N \omega_{sn} = x_{2s}$  denote the column sum for location  $s$ . Hence  $x_{2s}$  measures the impact of a Covid-19 shock ( $v_{st-2}$ ) in period  $t-2$  on the total number of infectives at the end of period  $t-1$ . It measures the degree to which location  $s$  exports contagion in the short-run to all locations including itself. The  $s$ 'th column sum ( $x_{3s}$ ) of  $\Omega^2$  measures the degree to which location  $s$  exports contagion following a Covid-19 shock in period  $t-3$  ( $v_{st-3}$ ). Henceforth, let  $\chi_s(\Omega)$  denote a column sum operator for column  $s$  of a matrix such as  $\Omega$ .

Using the spectral decomposition for  $\Omega = ZHZ'$ , where  $H$  is a diagonal  $N \times N$  matrix of eigenvalues of  $\Omega$ , and  $Z$  denotes its matrix of eigenvectors with elements  $\zeta_{sn}$ , we may express  $\Omega^{j-1}$  as:

$$\Omega^{j-1} = ZH^{j-1}Z' \quad (8)$$

If  $k$  is stationary the eigenvalues must be less than 1, in which event  $\Omega$  converges to zero with  $j$ . Matters are different if  $k$  is nonstationary, which arises if at least one of the eigenvalues is at least 1. Equation (8) establishes that  $x_{js}$  depends on powers of the eigenvalues, which decrease with  $j$  in the stationary case and increase otherwise. Importantly, it also implies that  $x_s$  may be ranked by  $x_{2s}$  as demonstrated below.

In the stationary case, the long-term contagiousness of location  $s$  is defined by:

$$x_s = \sum_{j=1}^{\infty} x_{js} = \sum_{j=1}^{\infty} \chi_s(ZH^{j-1}Z') \quad (9)$$

which is convergent by definition. In the nonstationary case equation (9) is divergent.

Figure 3A is the heat map for outdegrees of  $\Omega$  in equation (7). It is the heat map for the outdegrees for infectives ( $k$ ) generated by the simulated counterpart to Figure 1B when  $\gamma = \lambda = 0$  and  $W$  is defined in terms of inverse distance instead of rook-contiguity. The outdegrees range between 1.45 and 1.533. They are smallest in the corners (periphery) and largest in the epicenter. An outdegree of 1.45 means that a unit shock to  $v_{t-1}$  increases total infectives ( $k$ ) in period  $t$  by 1.45. Since the direct effect of a unit shocks is 1, the indirect effect induced by contagion between and within locations is 0.45 in the corners of the lattice. At the epicenter of the lattice this contagion effect is 0.533. Notice that the heat map is symmetric. For example, locations with addresses row 1 columns 2 and 9, row 2 columns 1 and 10, row 9 column 1 and 10 and row 10 column 2 and 9 have outdegrees equal to 1.467, The closer to the epicenter the greater the outdegree. Centrality is the only reason why outdegrees differ because all locations share the same parameter values.

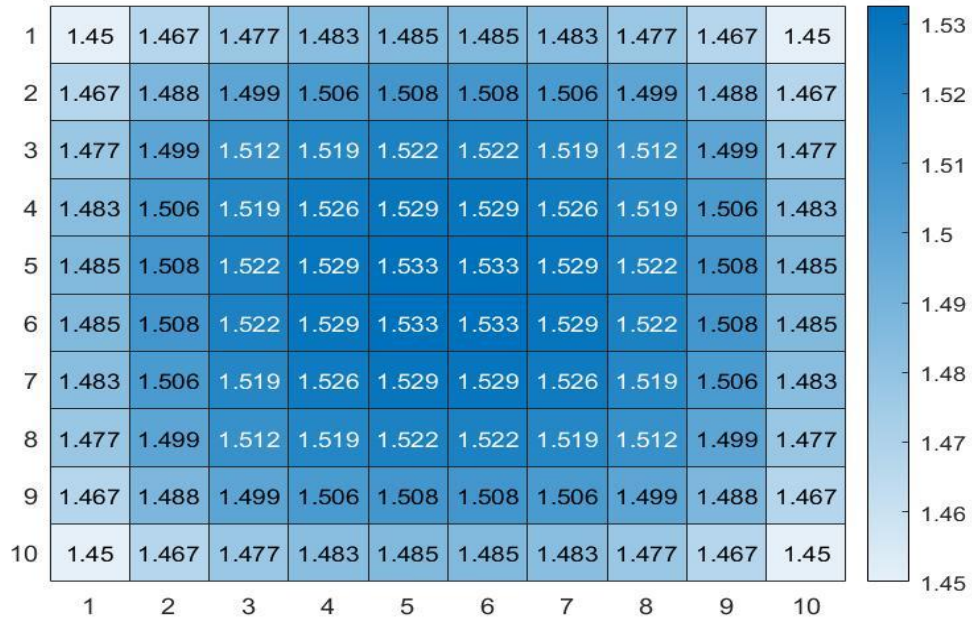
The symmetry of the heat map is induced by the shape or topology of the domain. For example, a triangular lattice would have generated an asymmetric heat map. The same pattern applies in panel B. The outdegrees refer to the effect of a unit shock to  $v_{t-1}$  after two periods. They are larger than in panel A because  $k$  is nonstationary, otherwise the outdegrees would have been smaller than in panel A. Notice that the ranks of the column sums are the same in panels A and B. The cumulative impulse response for corner locations is  $1.45 + 2.109 = 3.559$ . Contagion has increased from



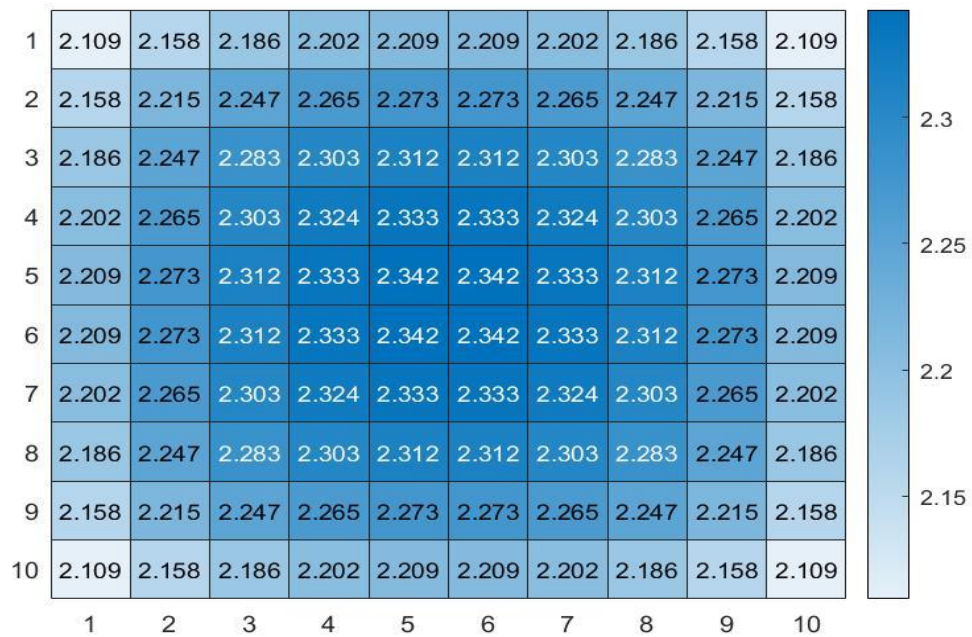
0.45 to 2.559. After a further period contagion increases by a further 3.078 (not shown). At the epicenter contagion is 6.447 after three periods.

**Figure 3 Heat Map: Outdegrees for Infectives**

**Panel A:  $\Omega$**



**Panel B:  $\Omega^2$**



Relaxing the restriction  $\Lambda = \Gamma = 0$  in equation (1) complicates matters because  $y$  is no longer recursive to  $k$ . Rewrite equation (5) as:

$$y_t = My_{t-1} + Fy_{t-2} + v_t \quad (10)$$

where  $M = \Phi + G + B$ ,  $F = -GB$  and  $v_t = A\varepsilon_t - \Phi A\varepsilon_{t-1} + B\varepsilon_{t-1}$ . The general solution to equation (10) is:

$$y_t = Qv_t \quad (11)$$

Where  $Q = (I - ML - FL^2)^{-1}$  and  $L$  is a temporal lag operator. Expanding the inverse gives the first terms as  $I + ML + (F + M^2)L^2 + (MF + M^3 + MFM)L^3$ . If  $y$  is stationary the coefficients of powers of  $L$  decrease towards zero. The instantaneous outdegree for location  $s$  with respect to a Covid-19 morbidity shock ( $\varepsilon_{st}$ ) is the  $s$ 'th column sum of  $A$ , i.e.  $\chi_s(A)$ . Its counterpart for a morbidity shock in period  $t-1$  is  $\chi_s(M) - \chi_s(\Phi A)$ . The Wold representation for  $y$  with respect to  $\varepsilon$  takes the form:

$$y_t = \sum_{j=0}^{\infty} C_j \varepsilon_{t-j} \quad (12)$$

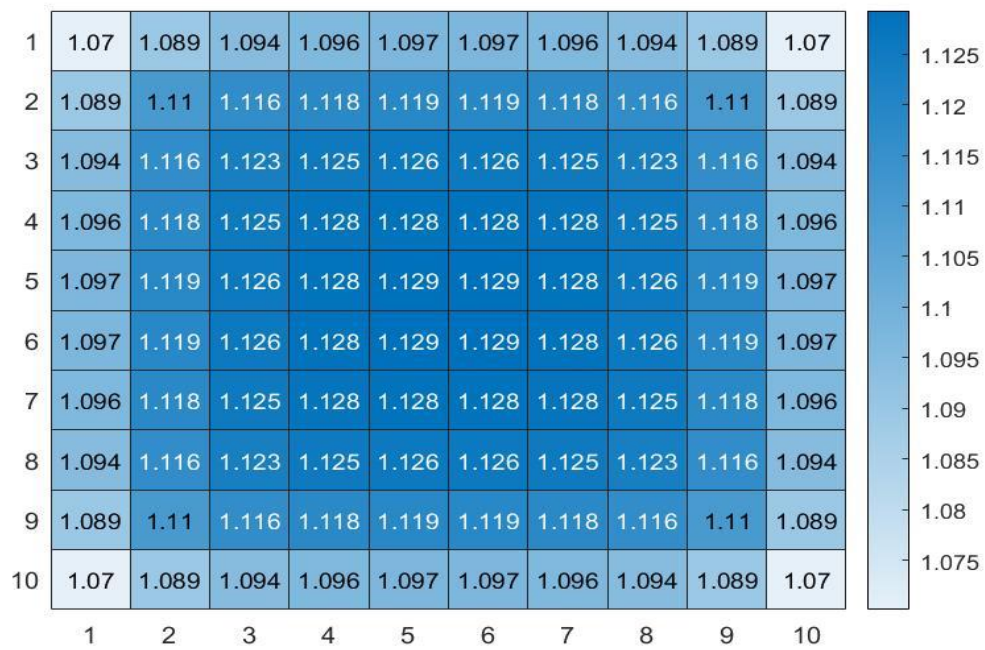
where  $C_j$  are  $N \times N$  matrices which increase with  $j$  if  $y$  is nonstationary, and tend to zero with  $j$  if  $y$  is stationary. We refer to the outdegrees of  $C_j$  as the  $j$ 'th order outdegree.

The heat maps for equation (12) are shown in Figure 4 with respect to unit shocks in  $\varepsilon_t$  and  $\varepsilon_{t-1}$  on  $y_t$ . The pattern in Figures 4 is the same as in Figures 3. Centrality matters. The ranks of outdegrees in panels A and B are the same. Note that the outdegree magnitudes in Figures 4 cannot be compared to those in Figures 3 because the latter refer to  $y$  while the former refer to  $k$ , and the data generating processes are different because in Figures 4,  $\gamma$  and  $\lambda$  revert to their values in Figure 1. However, in Figures 3 and 4  $y$  and  $k$  are nonstationary as is clearly apparent in Figure 1 and is reflected in the fact that the elements of  $C$  increase between panels in Figure 4.

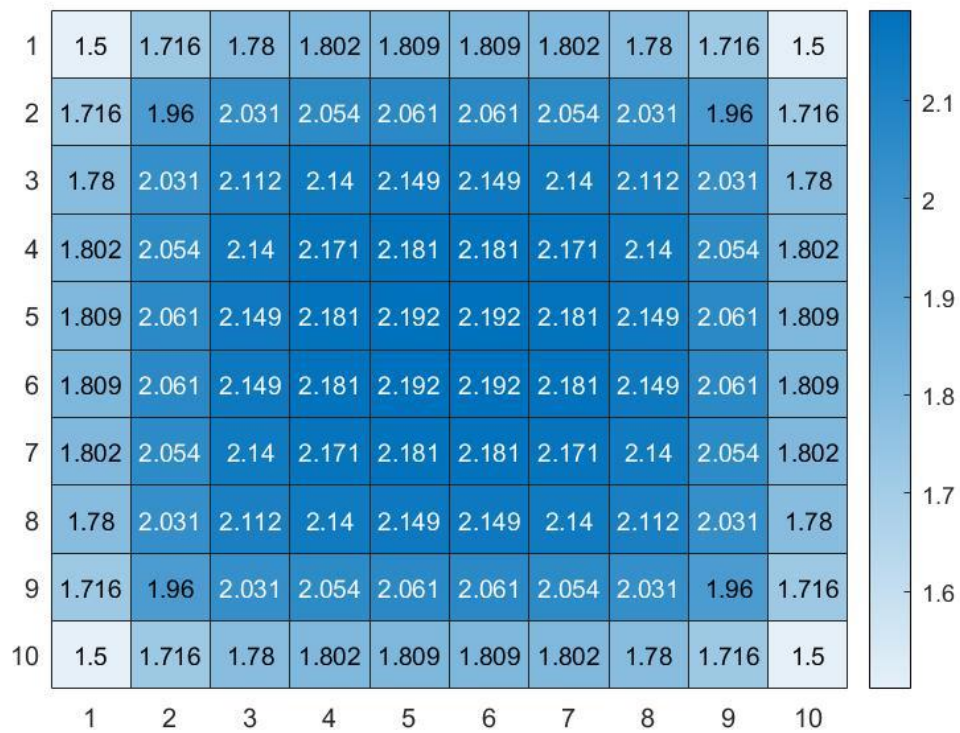
Panels A, B and C refer respectively to the heat maps for zero-order, first order and second order outdegrees. To obtain the cumulative outdegrees simply sum the outdegrees in panels A, B and C. For example at the epicenter the cumulative outdegree after three periods is 10.244, and in the periphery (corners) it is 6.652.

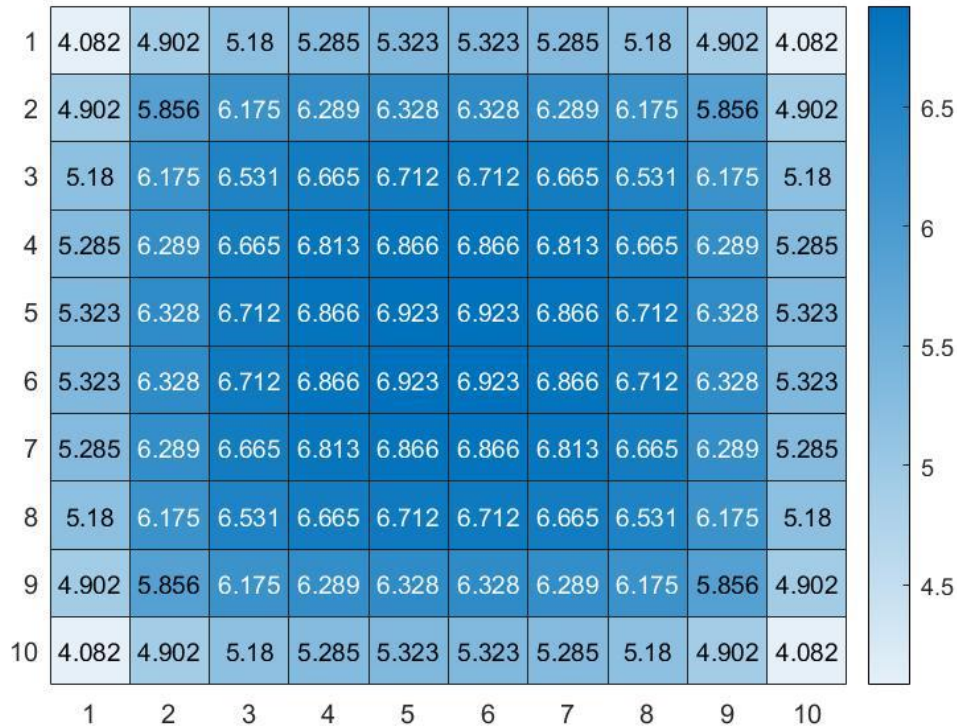
**Figure 4 Heat Map: Outdegrees for Morbidity (Equation 12)**

**Panel A:  $C_0$**



**Panel B:  $C_1$**



**Panel C:  $C_2$** 

Sensitivity analyses show with respect to  $\Omega$  that if  $\psi$  (spatial contagion rate) is increased in one location its outdegree remains unchanged (experiment 1 in the Appendix). The outdegrees for all other locations increase because if the location in question imports more morbidity, the others must export more. However, their outdegree ranks remain unchanged. Hence, the rank of the outdegree of the perturbed location decreases.

If  $\phi$  (time to recovery) is increased in one location its outdegree increases because its infectives remain contagious for longer, while the outdegrees in all other locations remain unchanged (experiment 2 in Appendix). If  $\pi$  (indigenous contagion rate) increases in one location its outdegree increases because its infectives are more contagious, but outdegrees elsewhere decrease (experiment 3) because the location in the experiments crowds out contagion elsewhere.

Since  $\Omega$  does not depend by definition on  $\lambda$  and  $\gamma$ , experiments involving these parameters are based on the outdegrees for the  $C$  matrices in equation (12) with baseline values presented in Figure 4. The latter are repeated for convenience in Table 1 (baseline). The final column in Table 1 refers to the cumulative outdegrees after

three periods. For example, in the corners of the lattice an additional case of morbidity infects 6.652 nationally after three periods.

In experiment 4  $\lambda$  (inertia in morbidity) is increased to 0.35 from 0.3 in column 1 row 6 (treated location). Since  $\lambda$  is a temporal autoregressive parameter, it has no effect on  $C_0$ , hence the instantaneous outdegree remains unchanged at its baseline value. After one period the outdegree of the treated location increases from 1.809 to 1.86 (via  $C_1$ ) but the other outdegrees remain unchanged in all locations. The increase in  $\lambda$  increases the propagation of morbidity within the treated location, as a result of which, it exports more Covid-19. After a further period ( $C_2$ ) the outdegrees decrease in experiment 4 relative to the baseline, as do the cumulative outdegrees ( $C_0 + C_1 + C_2$ ) due to complex roots in the dynamical system of contagion.

**Table 1 Outdegree Sensivity to  $\lambda$  and  $\gamma$**

	$C_0$	$C_1$	$C_2$	$C_0 + C_1 + C_2$
<i>Baseline</i>				
Corner	1.07	1.50	4.082	6.652
Epicenter	1.129	2.192	6.923	10.234
Treated location	1.097	1.809	5.323	8.229
<i>Experiment 4: <math>\lambda=0.35</math></i>				
Corner	1.07	1.5	3.304	5.874
epicenter	1.129	2.192	5.485	8.806
Treated location	1.097	1.86	4.394	7.351
<i>Experiment 5: <math>\gamma=0.5</math></i>				
Corner	1.088	1.668	3.863	6.619
Epicenter	1.135	2.207	5.478	8.820
Treated location	1.104	1.89	4.505	7.499

In experiment 5 the SAR coefficient for morbidity ( $\gamma$ ) is increased to 0.5 from 0.3 in the treated location. Since the SAR coefficient refers to the current period, the outdegrees increase instantaneously through  $C_0$ . After a further period the cumulative outdegrees continue to increase, but as in experiment 4 the final column in Table 4 is less than in the baseline.

If the domain of the lattice is expanded by two tiles so that the number of locations is increased from 100 to 144, the outdegrees increase especially on the edge and corners of the original lattice, but decrease slightly at the epicenter because the epicenter of the lattice is relatively remote from the expanded domain. Expanding the domain reduces centrality, as expected. Indeed, asymptotically centrality loses its importance as the domain is expanded to infinity. Also, the outdegrees on the expanded domain tend to be smaller than for the previous edge and corners (experiment 6).

Finally, the outdegrees depend on how  $W$  is specified; they are more sensitive to centrality if  $W$  is defined in terms of Euclidean distance rather than rook contiguity. Centrality matters less with rook contiguity because each location is directly connected to between two and four locations, whereas with distance locations at the epicenter are more directly connected than locations in the periphery.

The symmetry in Figures 3 and 4 stems from the assumption that the parameters in equations (1) and (2) are homogeneous across locations. In reality, these parameters are likely to be heterogeneous in which case the outdegree heat maps will not be symmetric. Consequently, outdegrees in the center may not be greater than in the periphery. Indeed, centrality may lose its salience. The outdegrees are an empirical matter depending on the estimates of the structural parameters in equations (1) and (2).

## 5. The Relation between Outdegrees and $R$

Epidemiologists use  $R$  as a measure of contagion rather than outdegrees. In this section we explore the relation between  $R$  and outdegrees, and explain why outdegree is a superior metric to  $R$  for operating traffic light policy. For these purposes, we use the 'overlapping generation method' (Beenstock and Xieer 2020) for calculating  $R$  in real time. Instead of equation (2) the number of infectives ( $k$ ) is calculated using the 'perpetual inventory' formula:

$$k_t = \sum_{j=1}^{\tau} y_{t-j} + v_{t-1} \quad (13)$$

where infectives are contagious for  $\tau$  periods, and in equation (1)  $\pi = R/\tau$ , i.e. infectives infect  $R/\tau$  susceptibles per period, while they remain infective. To fix ideas we assume that all other parameters in equation (1) are zero. Hence:

$$R_t = \frac{y_t}{\bar{y}_{t-1} + v_{t-1}} \quad (14)$$



Where  $\bar{y}$  denotes the mean of  $y$  over  $\tau$  previous periods. At the beginning of period  $t$   $v_{t-1}$  is known. During period  $t$   $y_t$  is observed. If  $u_t$  is assumed to be zero, equation (14) solves for the expected value of  $R$ , which varies by  $t$ . Notice that, as expected, equation (1) implies that  $R = 1$  when  $y$  is constant, and exceeds 1 if  $y$  increases.

Suppose, next, that there are two locations 1 and 2. Equation (13) applies in both locations to determine  $k_1$  and  $k_2$  in terms of  $y_1$  and  $y_2$  respectively, and  $\pi_1 = R_1/\tau$  and  $\pi_2 = R_2/\tau$ . Morbidity in locations 1 and 2 is:

$$y_{1t} = \pi_1 k_{1t} + \psi_1 k_{2t} + u_{1t} \quad (15a)$$

$$y_{2t} = \pi_2 k_{2t} + \psi_2 k_{1t} + u_{2t} \quad (15b)$$

Solving equations (15) for  $\pi_1$  and  $\pi_2$  given  $\psi_1$  and  $\psi_2$  implies that spatially adjusted  $R$ , denoted by  $R^*$ , in locations 1 and 2 are:

$$R_{1t}^* = R_{1t} - \tau\psi_1 \frac{\bar{y}_{2t-1}}{\bar{y}_{1t-1}} \quad (16a)$$

$$R_{2t}^* = R_{2t} - \tau\psi_2 \frac{\bar{y}_{1t-1}}{\bar{y}_{2t-1}} \quad (16b)$$

Equations (16) adjust standard measures of  $R$  for imports of contagion. If contagion within locations is greater than contagion between locations then, for example,  $\tau\psi_1 < R_2$ . Table 2 provides numerical illustrations for the relation between  $R$  and  $R^*$ . The standard measures of  $R_1$  and  $R_2$  are assumed to be 1.3 and 0.8. So it appears that  $R$  is greater in location 1. In row 1 this rank is reversed because location 2 exports contagion to location 1, hence spatially adjusted  $R$  in location 1 is less than in location 2. In row 2 the standard measure is correct because there is no trade in Covid-19. In row 3 spatially adjusted  $R$  is greater in location 1 than in location 2, but the difference has narrowed to 0.2 from 0.5. In row 4 the difference increases from 0.5 to 0.635.

$R$  penalizes locations, which happen to import contagion, while  $R^*$  takes account of the outdegree of exporters. In row 1 location 1 is penalized unfairly by  $R$  whereas location 2 is justly penalized by  $R^*$ .

**Table 2 The Relation between R, R\* and R#**

$\tau\psi_1$	$\tau\psi_2$	$\bar{y}_2/\bar{y}_1$	$R_1^*$	$R_2^*$	$R_1^\#$	$R_2^\#$
0.6	0	1.5	0.4	0.8	1.3	1.4
0	0	1.5	1.3	0.8	1.3	0.8
0.6	0.3	1	0.7	0.5	1.6	1.4
0.3	0.3	0.8	1.06	0.425	1.6	1.1

$R_1 = 1.3, R_2 = 0.8. \tau\psi_1 < R_2, \tau\psi_2 < R_1.$

Another way of looking at the same thing is to define  $y^*$  as indigeneous contagion plus exported contagion (instead of minus imported contagion). For location 1:

$$y_{1t}^* = (R_1 + \tau\psi_2)\bar{y}_{1t-1} \quad (17)$$

Let  $R_1^\# = R_1 + \tau\psi_2$  denote 'global R' for location 1, which is reported in Table 2. The rank of location 1 is the same for  $R^\#$  and  $R^*$ , but the differences are smaller in Table 2.

The counterparts to equations (16) and (17) in terms of outdegrees are obtained by substituting equation (13) into equations (15) for k in locations 1 and 2:

$$\begin{pmatrix} 1 - \pi_1 F(L) & -\psi_1 F(L) \\ -\psi_2 F(L) & 1 - \pi_2 F(L) \end{pmatrix} \begin{pmatrix} y_{1t} \\ y_{2t} \end{pmatrix} = \begin{pmatrix} u_{1t} + \pi_1 v_{1t-1} + \psi_1 v_{2t-1} \\ u_{2t} + \psi_2 v_{1t-1} + \pi_2 v_{2t-1} \end{pmatrix} \quad (18)$$

where  $F(L) = \sum_1^t L^j$ . Equation (18) solves for the impulse responses of  $y_1$  and  $y_2$  with respect to morbidity shocks ( $u_1$  and  $u_2$ ) and with respect to recovery shocks ( $v_1$  and  $v_2$ ). The coefficient matrix has  $2\tau$  eigenvalues through  $F(L)^2$ . In Table 3 we report the zero, first and second order outdegrees for locations 1 and 2 with respect to their morbidity shocks.



**Table 3 Outdegrees for Equation 18**

<b>Outdegree order</b>	<b>Location 1 (<math>u_1</math>)</b>	<b>Location 2 (<math>u_2</math>)</b>
0	1	1
1	$\pi_1 + \psi_2$	$\pi_2 + \psi_1$
2	$\pi_1(1 + \pi_1) + \psi_1(1 + \psi_2) + \psi_2(1 + \pi_1 + \pi_2)$	$\pi_2(1 + \pi_2) + \psi_2(1 + \psi_1) + \psi_1(1 + \pi_1 + \pi_2)$

If  $\pi$  is the same in both locations the difference between the first order outdegrees for location 1 relative to location 2 is  $\psi_2 - \psi_1$  (location 1 exports more contagion to location 2 than does location 2 export to location 1). The difference for the second order outdegrees is  $2\pi(\psi_2 - \psi_1)$ . Notice that the ranks of the outdegrees depend simply on the difference between  $\psi_2$  and  $\psi_1$ . If  $\psi$  is the same in both locations the outdegree difference is  $\pi_1 - \pi_2$  (1<sup>st</sup> order) and  $\pi_1(1 + \pi_1) - \pi_2(1 + \pi_2)$  (2<sup>nd</sup> order); the difference depends on the difference between  $\pi$ . Since e.g.  $\pi_1 = R_1/\tau$ , the relation between outdegrees and R is readily obtained.

## 6. Spiking

In section 3  $\varepsilon$  and  $e$  were assumed to be iid and their distributions symmetric across locations. This leaves outdegree as the sole criterion for operationalizing traffic light policy. It also means that morbidity cannot 'spike' because the probability of large morbidity shocks does not vary over time. In practice, the distribution of  $\varepsilon$  in particular may vary by location, and it may not be iid.

If the variance in location  $s$  is larger than in location  $j$ , the probability of drawing large lognormal morbidity shocks is obviously greater in  $s$  than in  $j$ . If the outdegrees in  $s$  and  $j$  are the same, common sense suggests that location  $s$  should be 'redder' than location  $j$ . The same would apply if the variances happen to be the same, but the distribution is more skewed in  $s$  than in  $j$ ; it has fatter right tails.

If  $\varepsilon$  is not iid this might happen for a number of reasons. First,  $\varepsilon$  is serially correlated; morbidity shocks are persistent. Persistence induces spiking because shocks propagate

over time. If persistence is greater in location  $s$  than in location  $j$ , all else the same, location  $s$  should be redder than location  $j$ . Second,  $\varepsilon$  is an ARCH process (the variance is conditionally autocorrelated, Kamalov and Thabta 2021); the unconditional variance is homoscedastic but the conditional variance is not. ARCH processes may induce spiking because the variance of  $\varepsilon$  increases before it returns to its unconditional counterpart. Larger variances increase the probability of drawing larger lognormal shocks. If the ARCH coefficient in location  $s$  is larger than in location  $j$ , location  $s$  should be redder. Third, if  $\varepsilon$  is a diffusion-jump process it will be characterized by spiking depending on the size of the jump and its arrival rate. If these parameters are greater in location  $s$  than in location  $j$ , all else given, location  $s$  should be redder.

Equation (19) is a 1<sup>st</sup> order autoregressive 'jump' model for  $\varepsilon$  in location  $s$  in which persistence varies directly with  $\rho > 0$ , the jump size is  $J > 0$ ,  $\kappa$  denotes its (Poisson) arrival rate, and  $w$  is an iid residual error:

$$\varepsilon_{st} = \rho_s \varepsilon_{st-1} + F(J_s, \kappa_s) + w_{st} \quad (19)$$

The 1<sup>st</sup> order ARCH model for  $\varepsilon$  is:

$$\sigma_{st}^2 = \alpha_s + \mu_s \varepsilon_{st-1}^2 \quad (20)$$

If  $\rho < 1$ ,  $J$ ,  $\kappa$  and  $\mu < 1$  are zero and  $\alpha_s = \alpha$  we revert to the symmetric iid case in section 3. The unconditional variance for  $\varepsilon$  in location  $s$  is  $\alpha_s / (1 - \mu_s)$ . Since these parameters are empirical matters, they may be estimated together with the structural parameters in equations (1) and (2). Locations with larger estimates of  $\rho$  etc are spikier and therefore redder. Estimation of time series models combining jump and ARCH processes have been discussed by Drost, Nijman and Werker (1998).

Equations (19) and (20) are spatially independent. If necessary, equation (19) may be specified as a spatial error model (SEM) and equation (20) as a spatial ARCH model (Beenstock and Felsenstein 2019).

## 7. Conclusions

We propose outdegree from graph theory as a sufficient statistic for measuring the contagiousness of locations for operating 'traffic light' policy as an alternative to national mitigation policy. This measure is applicable to any contagious disease and not just Covid-19. The outdegree for locations measure their contribution to national morbidity. Outdegree justly penalizes locations for the contagion that they propagate. By contrast the practice of calculating R for locations unfairly exonerates locations, which export contagion, and penalizes locations, which import contagion. Standard measures of R make traffic light policy accident prone. By contrast, traffic light policy based on outdegree make it efficient as well as just.

We draw six tentative policy highlights from the theoretical model. The first is that mitigation needs to be directed at exporting locations rather than importing locations. In practice public policy has tended to treat them as equal. Interventions such as mobility constraints and lockdowns have not distinguished between Covid-19 origins and destinations. The second relates to policy targeting. Mitigation policy needs implementation at a high level of granularity that is politically and practically feasible. Interventions that are too granular run the risk of being challenged in the courts on the basis of unjust discrimination. Also, highly granular spatial units such as census tracts may not be practical for implementation because they cut across administrative boundaries, which are less granular. Third, policy prescriptions for super-spreading need to tread a fine line between stick and carrot incentives. As super-spreader locations are central nodes related to a finite number of dependent satellite locations, heavy-handed mediation is likely to have unanticipated knock-on effects on other (Covid-importing) locations.

Fourth, outdegrees are fixed in the theoretical model if the structural parameters do not change, implying that traffic light colors do not change over time. There is no traffic light mobility. In practice, traffic light coloring has been mobile, changing from green to red and back again within weeks. We see this dissonance as a result of R-based traffic light policy. R may change from week to week when outdegrees remain unchanged. There is an obvious danger of 'instrument instability' or delayed policy overkill. For example, the traffic light turns from red to green to alleviate a congestion but reverts to red before the effect of the change can take effect.

Frustrated drivers will no doubt recognize this phenomenon. In terms of traffic light policy for mitigating Covid-19 contagion, locations can change their color coding radically, going from green to red designations. However the policy response to this color change may only take effect when the new color designation is no longer relevant, inducing policy overkill and instrument instability. In contrast, outdegree theory predicts that traffic light coloring should be relatively stable.

Fifth, morbidity spikes more where the spiking parameters (ARCH, jump-size etc) happen to be larger. Although they are not hard-wired, these parameters are likely to be stable. Hence their contribution to traffic light shading is unlikely to be volatile. Here too, delayed spike chasing may induce instrument instability. These policy propositions may be assessed using econometric estimates of the SIR model and its model for morbidity shocks.

Sixth, if the factors that increase outdegrees can be identified at specific locations this provides the key for targeted policy prescriptions. For example, the outdegree of a location may happen to be large because of indigenous contagion in an importing location. Hence, mitigating contagion in the importing location will reduce the outdegree in the exporting location.

We conclude with reflections on bringing theory to data. Since outdegree is the column sum of propagation matrices in spatiotemporal models of contagion, the spatial econometric methodology for their estimation is readily available. Hence, to operationalize outdegree as the criterion for efficient traffic light policy design is relatively straightforward. Indeed, in this paper we have described how to derive outdegrees from spatiotemporal econometric models of contagion.

For reasons of transparency we have focused on the 'natural history' of Covid-19 spatial transmission (Beenstock and Dai 2020). In Figure 1 the natural history of Covid-19 is nonstationary. In reality the 'unnatural history' is mostly stationary and wave-like thanks to mitigation policy in 2020 and to vaccination policy in 2021. Mitigation policy was initially national or federal but subsequently specific locations were targeted through experiments with traffic light policy. In bringing theory to data, it will be essential to take mitigation and vaccination policy into consideration.

In the theoretical model space is represented by an orderly lattice. In reality space is messy; borders are political and social as much as physical. Also, real space looks

more like a jigsaw puzzle than a chessboard. This is critical as many spatially differentiated mitigation policies are contingent on social practices, cultural norms or administrative conventions unique to particular locations. Mask-wearing is a case in point: in certain locations this may be considered as acceptable and reasonable while in others it is met with opposition and resistance.

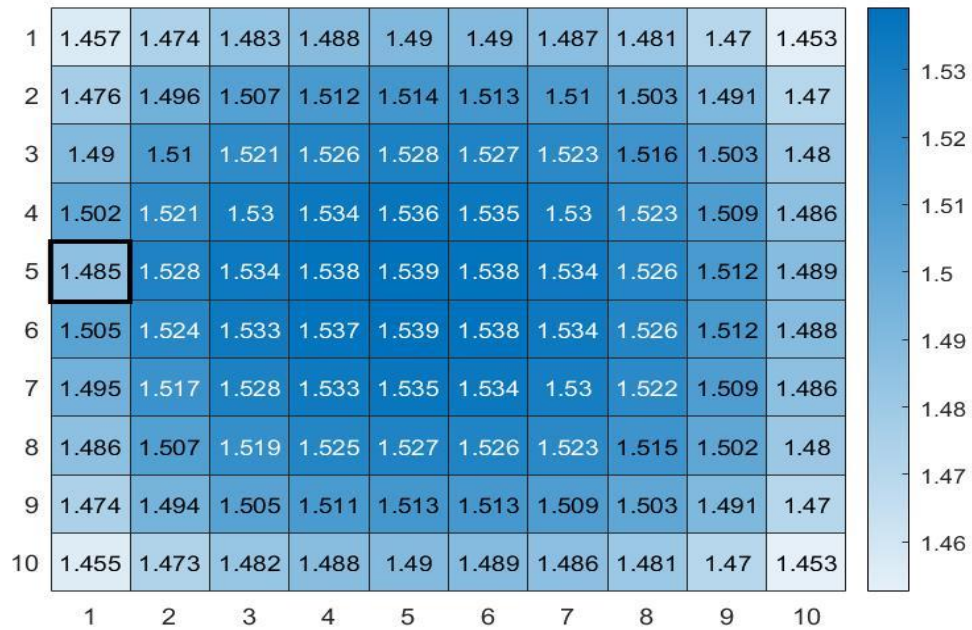
Econometric methods for estimating the 'spiking' model for morbidity innovations are also available. However, we suggest a two-stage procedure in which their distributions are initially assumed to be iid and symmetrical. If they are not, the parameter estimates of the SIR model are consistent but not efficient because the model is linear. If necessary, the spiking model for the morbidity innovations may be estimated in the second stage.

## Appendix: Sensitivity Analyses

### Experiment 1

Heat map for outdegrees for  $\Omega$  when  $\psi$  is increased from 0.2 to 0.8 in row 5 column

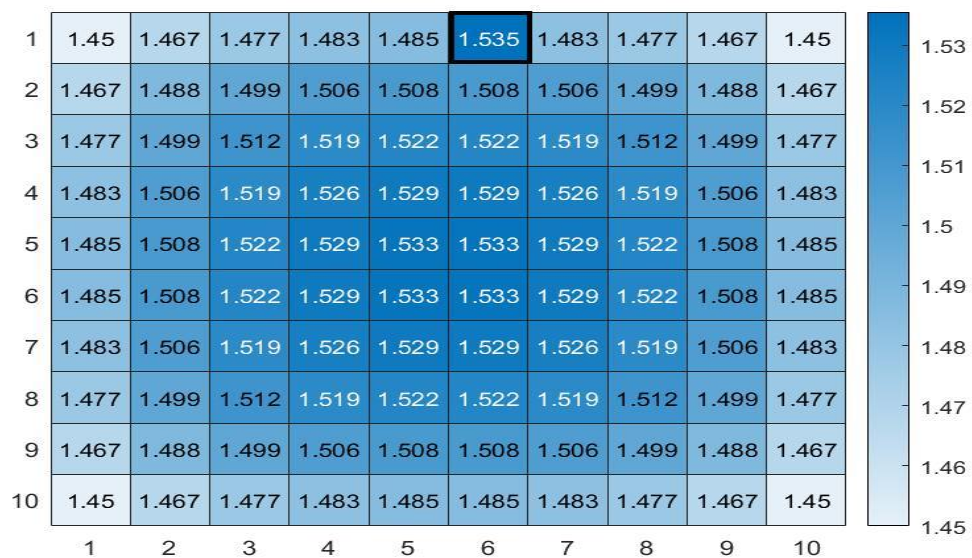
1. Outdegrees increase everywhere except for row 5 column 1.



### Experiment 2

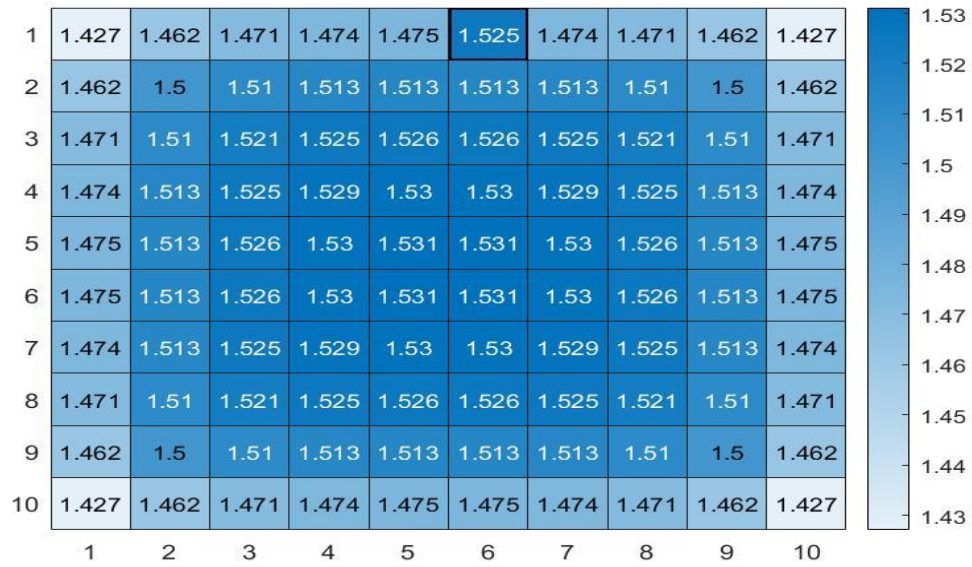
Heat map for outdegrees for  $\Omega$  when  $\phi$  is increased from 0.9 to 0.95 in row 1 column

6. Outdegree increases in row 1 column 6 and remain unchanged elsewhere.



### Experiment 3

Heat map for outdegrees for  $\Omega$  when  $\pi$  is increased from 0.4 to 0.45 in row 1 column 6. Outdegree increases in row column 6 and decrease everywhere else.



### Experiment 4

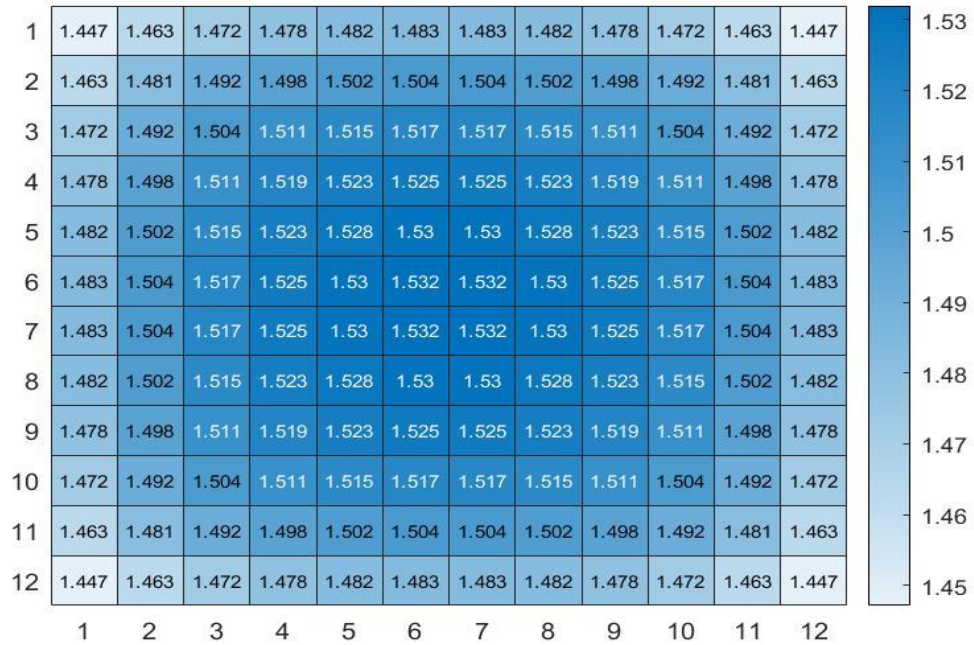
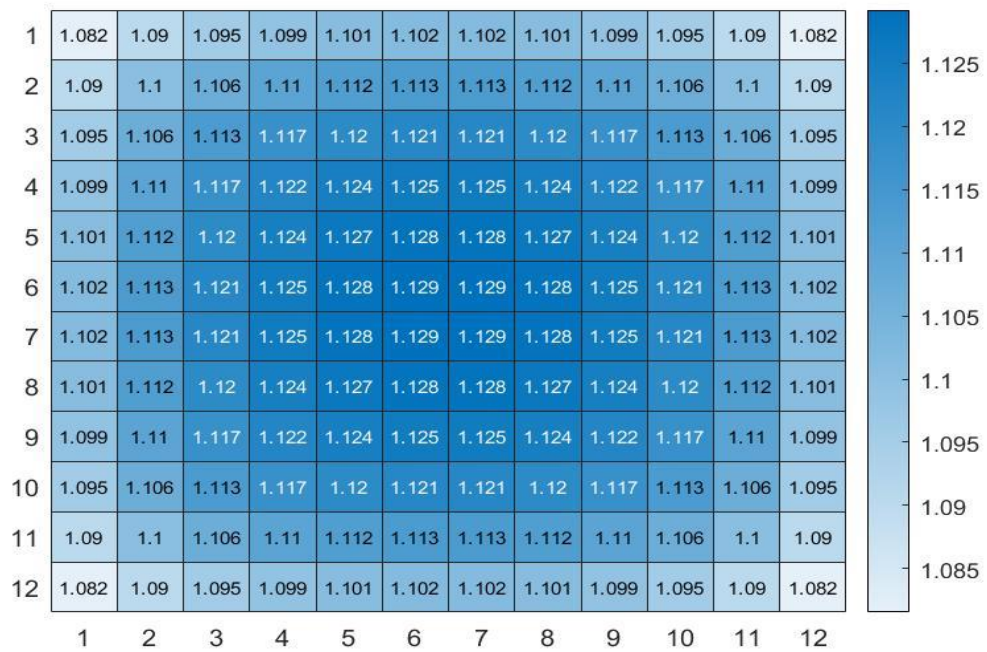
$\lambda$  is increased from 0.3 to 0.35 in row 1 column 6. See Table 1 in text.

### Experiment 5

$\gamma$  is increased from 0.3 to 0.5 in row 1 column 6. See Table 1 in text.

### Experiment 6

Expand domain to 12x12 lattice. Heat maps for column sums of  $\Omega$  and  $C_1$ .

$\Omega$ 

 $C_1$ 




## References

- Alvarez, F., Argente, D.O. and Lippi, F. (2020) A simple planning problem for COVID-19 lockdown, *Covid Economics* 14.
- Anderson, L. and van Wincoop, E. (2003) Gravity with Gravitas: A Solution to the Border Puzzle, *American Economic Review*, 93, 170-192.
- Argente, D.O., Chang-Tai, H. and Lee, M. (2020) The cost of privacy: welfare effect of the disclosure of COVID-19 cases. NBER Working Paper 27220  
<http://www.nber.org/papers/w27220>
- Beenstock, M. and Felsenstein, D. (2019) *The Econometric Analysis of Non-Stationary Spatial Panel Data*, Springer Nature, Switzerland.
- Beenstock, M. and Dai, X. (2020) The natural and unnatural histories of Covid-19 contagion, *Covid Economics*, 10, 92-120.
- Birge, J.R., Candogan, O. and Feng, Y. (2020), Controlling epidemic spread: reducing economic losses with targeted closures. Becker-Friedman Institute Working Paper No. 2020-57. [https://bfi.uchicago.edu/wp-content/uploads/BFI\\_WP\\_202057-1.pdf](https://bfi.uchicago.edu/wp-content/uploads/BFI_WP_202057-1.pdf)
- Cheshire, J. and Singleton, A. (2020) How England's complicated political geography is confusing coronavirus rules, *The Conversation*, December,  
<https://theconversation.com/how-englands-complicated-political-geography-is-confusing-coronavirus-rules-152036>
- Connexion France (2020) <https://www.connexionfrance.com/Practical/Your-Questions/Which-departments-in-France-are-low-risk-for-coronavirus>
- Diestel, R. (2005) *Graph Theory*. 3<sup>rd</sup> edition, Springer-Verlag, Berlin.
- Drost, F.C., Nijman, T.E. and Werker, B.J.M. (1998) Estimation and testing in models containing both jumps and conditional heteroscedasticity. *Journal of Business and Economic Statistics*, 16: 237-243.
- ECDC (2021) <https://www.ecdc.europa.eu/en/covid-19/situation-updates/weekly-maps-coordinated-restriction-free-movement>
- Fajgelbaum, P., Khandelwal, A., Kim, W., Mantovani, C. and Schaal, E. (2020), Optimal lockdown in a commuting network, NBER Working Paper 27441.  
[https://www.nber.org/system/files/working\\_papers/w27441/w27441.pdf](https://www.nber.org/system/files/working_papers/w27441/w27441.pdf)
- Gatto, M., Bertuzzo, E., Mari, L., Miccoli, S., Carraro, L., Casagrandi, R. and Rinaldo, A. (2020) Spread and dynamics of the COVID-19 epidemic in Italy: effects of emergency containment measures, *Proceedings of the National Academy of Sciences* 117(19):10484–10491
- Giannone, E., Paixão, N. and Pang, X. (2020) The geography of pandemic containment, *Covid Economics*, 52, 68-95.

Glaeser, E., Gorbach, C. and Redding, S.J. (2020) How much does COVID-19 increase with mobility? Evidence from New York and four other U.S. cities, *Journal of Urban Economics*, <https://doi.org/10.1016/j.jue.2020.103292>

GOVUK (2020) <https://www.gov.uk/government/speeches/review-of-local-restriction-tiers-17-december-2020>

HUGIS (2020) Normalized Accumulated Covid-19 Cases in Israel by Statistical Area, <https://hugis.maps.arcgis.com/apps/webappviewer/index.html?id=c470da7df01f44f4b6c0706dc238071f>

Kamalov, F. and Thabta, F. (2021) Forecasting Covid-19: SARMA – ARCH approach. *Health and Technology*, <https://doi.org/10.1007/s12553-021-00587-x>.

Krisztin, T., Piribauer, P. and Wögerer, M. (2020) The spatial econometrics of the coronavirus pandemic, *Letters in Spatial and Resource Sciences* 13, 209–218

Meenagh, D., Minford, P., Wickens, M. and Xu, Y. (2019) Testing DSGE Models by Indirect Inference: a Survey of Recent Findings *Open Economies Review*, 30, 593–620.

Mitze, T. and Kosfeld, R. (2021) The propagation effect of commuting to work in the spatial transmission of Covid-19, *Journal of Geographic Systems* <https://doi.org/10.1007/s10109-021-00349-3>

MoH (2020b) Traffic Light Instructions to Local Authorities, Ministry of Health and Homeguard Command, IDF [https://www.themarket.com/embeds/pdf\\_upload/2020/20200830-160844.pdf](https://www.themarket.com/embeds/pdf_upload/2020/20200830-160844.pdf)

MoH (2020a) Traffic Light Model <https://govextra.gov.il/ministry-of-health/magen-israel/traffic-lights-model/>

Monras, J. (2020) Some thoughts on COVID-19 from a labour mobility perspective: from ‘red-zoning’ to ‘green-zoning’, *VoxEU.org*, 25 March.

NZGOV(2020) <https://Covid19.govt.nz/alert-system/>

Oliu-Barton, M., Pradelski, B.S.R. and Attia, L. (2020), Exit strategy: from self-confinement to green zones, Esade – Center for Economic Policy & Political Economy, Policy insight No. 6, April. [https://www.esade.edu/itemsweb/wi/research/ecpol/EsadeEcPol\\_Insigh6\\_Exit\\_Strategy.pdf](https://www.esade.edu/itemsweb/wi/research/ecpol/EsadeEcPol_Insigh6_Exit_Strategy.pdf)

Prem, K., Liu, Y., Russell, T. W., Kucharski, A. J., Eggo, R. M., and Davies, N. (2020). The effect of control strategies to reduce social mixing on outcomes of the COVID-19 epidemic in Wuhan, China: A modelling study. *Lancet Public Health*, 5, 261-270. [https://doi.org/10.1016/S2468-2667\(20\)30073-6](https://doi.org/10.1016/S2468-2667(20)30073-6).

Warren, G.W., Lofstedt, R. and Wardman, J.K. (2021) COVID-19: the winter lockdown strategy in five European nations, *Journal of Risk Research*, 24 (3-4) <https://doi.org/10.1080/13669877.2021.1891802>

Wieland, T. (2020) Flatten the curve! Modeling SARS-CoV-2/COVID-19 growth in Germany on the county level. *REGION* 7(2):43–83.

Yamamoto, N. Jiang, B. and Wang, H. (2021) Quantifying compliance with COVID-19 mitigation policies in the US: a mathematical modeling study. *Infectious Disease Modelling*, 6, 503-515

Zhu, M., Guo, X., and Lin, Z. (2017). The risk index for an SIR epidemic model and spatial spreading of the infectious disease. *Mathematical Biosciences and Engineering*, 14, 1565-1583.